Fusion Engineering and Design 223 (2026) 115552

Contents lists available at ScienceDirect

Fusion Engineering and Design

journal homepage: www.elsevier.com/locate/fusengdes

Mathematical modeling and design of a microwave polarizer for DTT ECRH applications

Sofia Bertolami [a,*], Franco Di Paolo [a], Alessandro Bruschi [b], Francesco Fanale [b], Alessandro Moro [b], Saul Garavaglia [b], Gustavo Granucci [b,c], Afra Romano [c,d], Alessandro Simonetto [b]

[a] University of Rome Tor Vergata, Department of Electronic Engineering, Via del Politecnico 1, Rome, 00133, Rome, Italy
[b] Institute for Plasma Science and Technology-CNR, Via Roberto Cozzi 53, Milan, 20125, Italy
[c] DTT S.C.a r.l, Via Enrico Fermi 45, Frascati (RM), 00044, Italy
[d] ENEA, Fusion and Nuclear Safety Department, Via Enrico Fermi 45, Frascati (RM), 00044, Italy

ARTICLE INFO

Keywords:
Polarizer
ECRH
DTT
Nuclear fusion
Fusion engineering
High power microwave sources

ABSTRACT

In an Electron Cyclotron Resonance Heating (ECRH) system, to efficiently couple the signal power to the plasma, the signal wave polarization must be accurately matched to the plasma conditions at the plasma boundary. However, the millimeter-wave radiation from the power source (gyrotron) is normally linearly polarized: consequently, some kind of polarization matching is required. This study focuses on the design of a grating polarizer with sinusoidal grooves for the 170 GHz ECRH system, with an application specifically intended for the Divertor Tokamak Test (DTT), currently under construction in Frascati, Italy. To enable the generation of all possible output polarization states, a pair of polarizer mirrors will be employed and integrated into the Quasi-Optical (QO) transmission line connecting the gyrotrons to the Electron Cyclotron (EC) waves launchers. The primary objective of this study is to describe an analytical tool capable of providing detailed insights into the polarization characteristics of the reflected electric field resulting from the interaction between the incident wave and the polarizer. Additionally, the proposed program tool calculates the precise combinations of rotation angles required for the polarizers to achieve the desired output polarization states. The accuracy and reliability of the model's prediction have been validated by comparing them with simulations conducted using commercial electromagnetic software.

1. Introduction

Nuclear fusion is studied as a possible source of carbon-dioxide-free energy, thereby reducing greenhouse gas pollution that alters the climate and threatens Earth's life [1,2]. In a magnetically confined plasma nuclear fusion device, Electron Cyclotron Resonance Heating (ECRH) is essential for supplying the auxiliary heating needed to attain the conditions requisite for fusion reactions. The Divertor Tokamak Test (DTT) facility, currently under construction in Frascati (Italy), is designed to investigate alternative power-exhaust solutions [3]. A huge amount of external additional heating of 45 MW is required to achieve values of power at the separatrix comparable with future relevant fusion devices like DEMO. The primary contributor is the Electron Cyclotron Resonance Heating (ECRH) system, which will supply 28.5 MW to the plasma [4–6]. The power source used mainly for ECRH is the gyrotron [7–9], a vacuum Electronic device capable of operating on the D- or G-band, giving MW of power. Solid-State Power Amplifiers (SSPA) can reach such operating frequencies [10,11], but the required MW of power cannot be obtained even considering the low-loss waveguide combiners [12–15]. Another potential solution could be the use of High-Power Microwaves (HPM) sources capable of exceeding the gyrotron power [16–18]; however, they are currently unable to achieve the required operating frequencies. In addition, Free-Electron Lasers (FELs) [19–21] are being considered as potential substitutes for gyrotron sources of ECRH because of their ability to generate tunable high-power radiation at millimeter and submillimeter wave frequencies. However, the utilization of FELs in ECRH systems is currently limited by several factors. Indeed, the conventional pulse length of FELs is restricted to a few seconds, which is not sufficient for steady-state or long-pulse plasma operations. In addition, the technical complexity, size, and high fabrication and operation costs of FEL systems further restrict their usability for future broad applications on fusion devices.

* Corresponding author.
E-mail address: sofia.bertolami@uniroma2.it (S. Bertolami).

https://doi.org/10.1016/j.fusengdes.2025.115552
Received 7 August 2025; Received in revised form 7 November 2025; Accepted 29 November 2025
Available online 3 December 2025

Thus, gyrotrons are still the optimum and most appropriate source of ECRH in current and near-term fusion research.

In the DTT facility, the ECRH power will be delivered by 4 clusters, each incorporating 8 gyrotrons, whose Gaussian beams will be transmitted by a Quasi-Optical Multi-Beam transmission line to the antennas that will be placed in the DTT sector. The Radio-Frequency (RF) power generated by the gyrotrons is transported through a sequence of flat and focusing mirrors, integrated within a vacuum envelope, and is injected into the plasma via a pair of mirrors, one fixed and one steerable, located in the port plug of each launcher. In this transmission line [22,23], a couple of grooved metallic mirrors adapt the wave polarization to all possible plasma experiment requirements. Indeed, the polarization of the injected wave must be matched to the plasma to attain proper power absorption and avoid unwanted reflection or mode conversion. These grooved metallic mirrors induce a phase difference between orthogonal wave components, enabling the transformation of an incoming wave into an arbitrary polarization state. The typical approach relies on the combination of two grating polarizers: a linear polarizer and an elliptical polarizer. However, given the promising results, particularly in terms of ohmic losses, reported in [24], for the design of the DTT transmission line, the combination of two elliptical polarizer mirrors as a universal polarizer has been investigated.

This work explores the theoretical design and simulation of a sinusoidal grating elliptical polarizer for the DTT 170 GHz ECRH system.

The following second section presents the fundamental concepts needed to understand the principle of device operation. The theory of diffraction is then explored, with particular attention to the method used to solve the basic equations that describe its behavior and the program workflow.

The third section is dedicated to the design of the polarizer, detailing the relationship between incident and reflected waves, along with the resulting rotation angle and ellipticity.

In the fourth section, the results of the theoretical model are presented and validated by comparison with electromagnetic simulation data.

The fifth section analyzes the performance of the system resulting from the combination of two polarizers, highlighting the importance of the results obtained.

Finally, the sixth section collects the main conclusions of the work.

2. Grating polarizer: definition and analysis

A detailed model of a grating polarizer, including incident (E_i) and reflected (E_r) electric field components, is illustrated in Fig. 1; k_i is the incident wave vector while k_r is the reflected wave vector. The mirror is characterized by a periodic corrugation, defined by a specific depth and period. The mirror can also rotate around its y-axis at an angle defined as Φ. This rotation allows for variation of the polarization of the output electric field. To guarantee that only the zero-order mode propagates and prevent Bragg scattering in all directions, the period p of the profile of the polarizer must meet the following requirement.

$$p < \frac{\lambda}{1 + \sin\theta \cos\Phi} \tag{1}$$

In (1), λ is the wavelength, θ is the angle of incidence, and Φ is the mechanical rotation angle of the polarizer. The incident electric field can be decomposed into three components: two in the mirror plane, E_{fast} (TE mode), and E_{slow} (TM mode), and one perpendicular to the mirror plane. If we assume that the groove width is small enough, the electric field component parallel to the grooves will not penetrate the grooves significantly, while the perpendicular component will reach the bottom of the grooves, where it will be reflected [25]. This phenomenon will therefore introduce a phase difference between these two electric field components, which we will denote by τ. This phase difference is related only to the field components in the mirror plane [26].

To calculate this value, it is necessary to solve the integral method of vector theory of diffraction gratings [27].

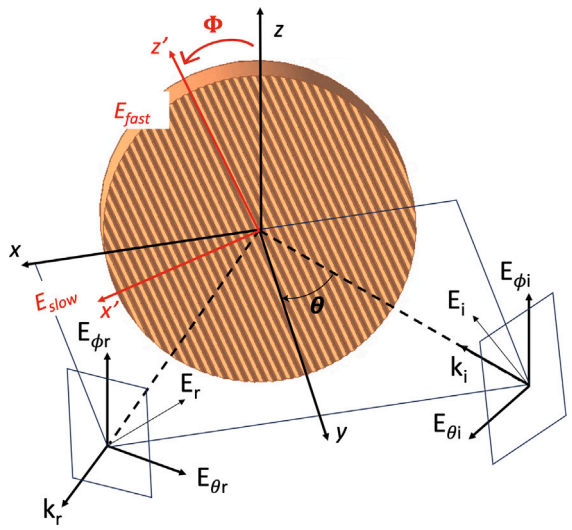

Fig. 1. Schematic diagram of the grating polarizer and geometric relationship between incident (E_i) and reflected electric field (E_r). The angle of incidence is θ and the rotation angle of the polarizer is Φ.

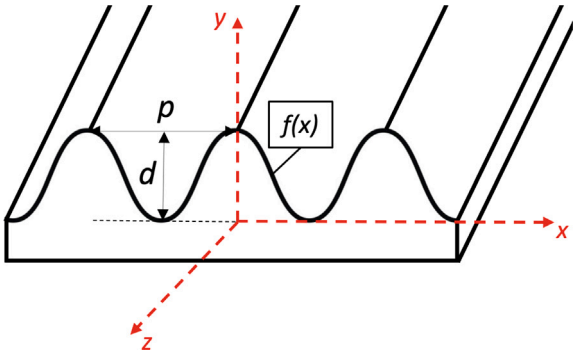

Fig. 2. Sinusoidal profile of the polarizer. The period of the corrugation is p, while the depth of the corrugation is d. $f(x)$ is the profile function chosen for the polarizer mirror.

2.1. Theory of diffraction gratings

The first step consists of defining the periodic profile that characterizes the corrugations of the polarizer. In the present analysis, a sinusoidal profile is assumed as a representative case, together with its associated coordinate system, as illustrated in Fig. 2. If we now consider a generalized incident plane wave interacting with the chosen periodic profile, it is possible to represent the reflected electric field of the TE mode and the magnetic field of the TM mode, following the theory of diffraction gratings, as follows:

$$F(x,y) = \sum_{n=-\infty}^{\infty} B_n e^{ik_{xn}x + ik_{yn}y} \tag{2}$$

$$k_n = \frac{2n\pi}{\lambda} \tag{3}$$

$$k_{xn} = k_n \sin\theta \tag{4}$$

$$k_{yn} = \sqrt{k_n^2 - k_{xn}^2} \tag{5}$$

where B_n can refer to the coefficients of the TE or TM modes, λ is the wavelength, θ is the angle of incidence, and n is the order of diffraction. In this formulation, the function F(x,y) represents the spatial dependence of the reflected field components across the x- and

y-directions. The reflected electric and magnetic field components can therefore be expressed as:

$$E_r(x,y,z) = |E_i(x,y,z)| \cdot F(x,y) \tag{6}$$

$$H_r(x,y,z) = |H_i(x,y,z)| \cdot F(x,y) \tag{7}$$

The coefficients of the TE mode can be determined following the equation:

$$B_{TE,n} = \int_0^p \frac{\Phi(x)}{2ipk_{yn}} e^{-ik_{xn}x - ik_{yn}f(x)}\,dx \tag{8}$$

where

$$\Phi(x) = 2\Phi_0(x) + 2\int_0^p N(x,x')\Phi(x')\,dx' \tag{9}$$

$$\Phi_0(x) = -ik(\cos\theta + f'(x)\sin\theta)e^{(ikx\sin\theta - ikf(x)\cos\theta)} \tag{10}$$

$$N(x,x') = \sum_{n=-\infty}^{\infty} \frac{1}{2p}[sign(f(x) - f(x')) - \frac{k_{xn}}{k_{yn}}f'(x)] \; e^{ik_{xn}(x-x') + ik_{yn}|f(x)-f(x')|} \tag{11}$$

Here, $f(x)$ represents the grating function utilized in the polarizer design, while $f'(x)$ is the first-order derivative of the profile function. The sign function is defined such that $sign(g(x))$ equals -1 when $g(x) < 0$ and equals 1 when $g(x) > 0$. In the previous equations, k is the wavenumber defined as $\frac{2\pi}{\lambda}$. Again, the coefficients of the TM mode are established by the following equation:

$$B_{TM,n} = \int_0^p \frac{\Psi(x)}{2p}(1 - \frac{k_{xn}}{k_{yn}}f'(x))e^{-ik_{xn}x - ik_{yn}f(x)}\,dx \tag{12}$$

where

$$\Psi(x) = 2\Psi_0(x) + 2\int_0^p N(x,x')\Psi(x')\,dx' \tag{13}$$

$$\Psi_0(x) = e^{ikx\sin\theta - ikf(x)\cos\theta} \tag{14}$$

$$N'(x,x') = \sum_{n=-\infty}^{\infty} \frac{1}{2p}[sign(f(x) - f(x')) - \frac{k_{xn}}{k_{yn}}f'(x)] \; e^{ik_{xn}(x-x') + ik_{yn}|f(x)-f(x')|} \tag{15}$$

After calculating the coefficients $B_{TE,n}$ and $B_{TM,n}$, it is possible to derive τ as follows:

$$\tau = arg(B_{TE,0}) - arg(-B_{TM,0}) \tag{16}$$

Eqs. (9) and (13) are formulated as Fredholm integral equations, which pose significant challenges in terms of solvability.

2.2. Numerical method and program workflow

The polarization characteristics of the reflected wave are determined primarily by the geometry of the chosen profile, such as depth (d) and period (p), angle of incidence (θ), and rotation angle (Φ). Generally, non-rectangular grooves with smooth edges are utilized to improve the power handling capabilities of grating polarizers in high-power ECRH systems, particularly those that operate at megawatt power levels [28]. To address Fredholm integral equations, numerous analytical techniques have been devised over the years, including the Coordinate Transformation Method (C-Method) [29], Rigorous Coupled Wave Analysis [30], and the Integral Point Matching Method (IPMM) [27]. This last method is recognized for its intuitive nature and, consequently, simple numerical implementation; for this reason, it is the most frequently employed. The core concept involves discretizing the previously discussed equations on the selected grating profile, thereby generating a set of linear equations. These linear equations can be subsequently resolved using various numerical techniques to determine the diffraction coefficients of interest. Despite its intuitive and rigorous characteristics, this method often necessitates extensive computations that are not easily addressed, and convergence issues may frequently occur. For these specific reasons, it was decided to solve the mathematical problem of phase shift calculation using the Integral Staggered Point Matching Method (ISPMM) described in [31]. The precision of the method is also demonstrated by comparing the results obtained with other methods mentioned above, such as the C-Method and IPMM. The promising results, along with the ease of integration into mathematical software, let us choose ISPMM.

The analytical program was implemented using MathCad [32], taking advantage of its matrix-oriented environment. A sinusoidal grating profile was selected, but it was parameterized so that the program was as general as possible. The profile function *f(x)*, the corrugation depth (d) and period (p), the wavelength (λ), and the angle of incidence (θ) can be input by the user. Once the basic input parameters are defined, the program discretizes the grating period in m points and then simultaneously applies two numerical integration rules: the trapezoidal rule for the x points and the midpoint rule for the x' points.

$$x_j = \frac{(j-1)p}{m-1}(1 \le j \le m) \tag{17}$$

$$x'_r = \frac{(2r-1)p}{2m-2}(1 \le r \le m-1) \tag{18}$$

This discretization technique avoids the convergence issues that are typically associated with the Fredholm integral equation. Then (9) and (13) were reformulated as follows:

$$\Phi(x_j) = 2\Phi_0(x_j) + \sum_{r=1}^{m-1} \frac{2p}{m-1} N(x_j, x'_r)\Phi(x'_r) \tag{19}$$

$$\Psi(x'_r) = 2\Psi_0(x'_r) + \sum_{j=1}^{m} \frac{C_j p}{m-1} N(x'_r, x_j)\Psi(x_j) \tag{20}$$

In (18) $C_1 = C_n = 1$ and $C_j = 2$ for $(2 \le j \le m-1)$.

These choices reduce the problem to the solution of systems of linear equations. After discretizing the Fredholm integrals, the coefficients $B_{TE,n}$ and $B_{TM,n}$ can be computed by solving the Eqs. (8) and (12) in their discrete form as follows:

$$B_{TE,n} = \frac{step}{2ip}\sum_{j=1}^{m} \frac{\Phi(x_j)}{k_{yn}} e^{-ik_{xn}x_j - ik_{yn}f(x_j)} \tag{21}$$

$$B_{TM,n} = \frac{step}{2p}\sum_{r=1}^{m-1} \Psi(x'_r)(1 - \frac{k_{xn}}{k_{yn}}f'(x))e^{-ik_{xn}x'_r - ik_{yn}f(x'_r)} \tag{22}$$

In the previous equations, the value of the *step* was chosen as $\frac{p}{m-1}$.

Once these coefficients are known, the calculation of the phase shift is straightforward.

The workflow of the developed program is presented in Fig. 3.

3. Design of the elliptical polarizer

As previously mentioned, for the design of the transmission line setup intended for DTT, a combination of two elliptical polarizer mirrors has been studied first, before addressing the conventional pairing of a linear and an elliptical polarizer. This choice was made to create a universal polarizer capable of producing any desired output polarization state. Taking into account the geometric model and the coordinate system illustrated in Fig. 1, one can derive the relationship between incident and reflected fields as follows:

$$\begin{bmatrix} E_{\theta_r} \\ E_{\phi_r} \end{bmatrix} = \begin{bmatrix} \cos\xi & -\sin\xi \\ \sin\xi & \cos\xi \end{bmatrix} \begin{bmatrix} e^{i\tau/2} & 0 \\ 0 & e^{-i\tau/2} \end{bmatrix} \begin{bmatrix} \cos\xi & -\sin\xi \\ -\sin\xi & -\cos\xi \end{bmatrix} \begin{bmatrix} E_{\theta_i} \\ E_{\phi_i} \end{bmatrix} \tag{23}$$

Where $\xi = \arctan(\tan\Phi\cos\theta)$ and τ is the phase shift calculated by applying the ISPMM in our MathCad program. In the optical design of the DTT ECRH transmission system, the angle of incidence θ was set to 22.5°. This value is given as a system requirement by DTT and is chosen to reduce ohmic losses on polarizers, even if the developed

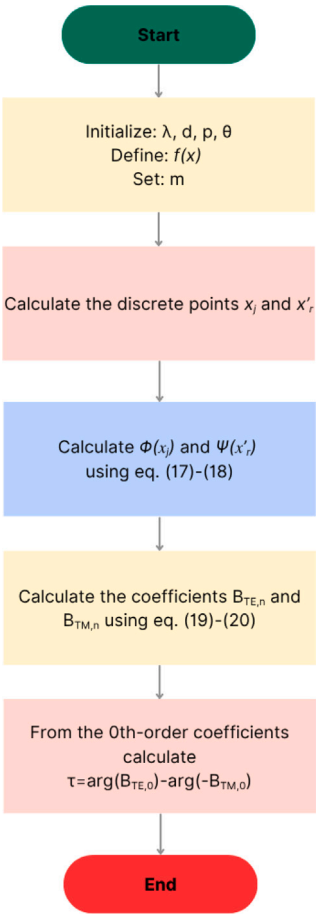

Fig. 3. Program workflow.

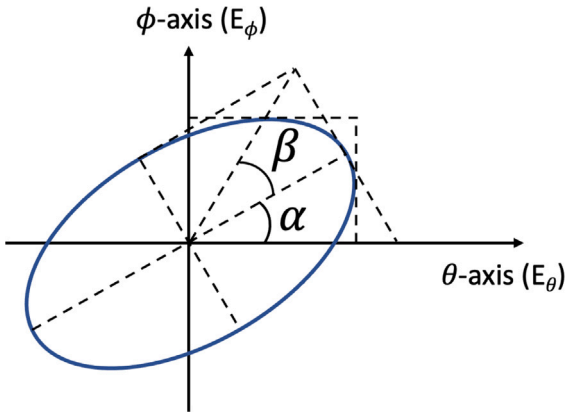

Fig. 4. Definition of the polarization parameters α and β in the chosen coordinate system. E_ϕ and E_θ are the ortogonal components of the electric field.

model remains applicable in more general cases. Also, it was assumed that both mirrors could rotate around their axes from 0 ° to 180° (0° ≤ Φ ≤ 180°) and that the angle of incidence is the same for both of them. Once the phase shift τ and the angle ξ are known, the reflected components of the electric field can be determined. From these components, it is possible to extract information regarding the output polarization. The key parameters for expressing the polarization of the electric field are two: the rotation angle (α) and the ellipticity (β), defined in Fig. 4.

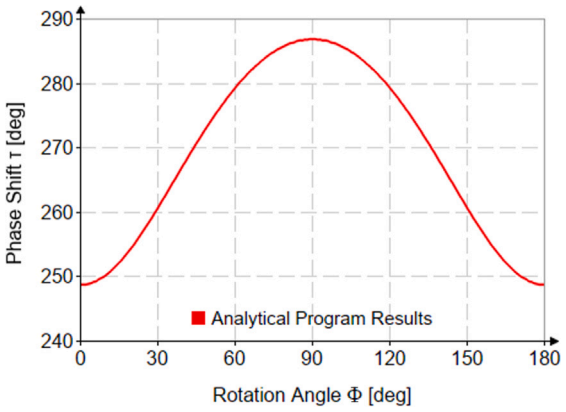

Fig. 5. Phase shift τ as function of the rotation angle Φ of the polarizer calculated with our mathematical program.

These two parameters can be analytically found by following the equations:

$$\tan(2\alpha) = \tan(2\gamma)\cos(\delta) \tag{24}$$

$$\sin(2\beta) = \sin(2\gamma)\sin(\delta) \tag{25}$$

For the previous equations, $\gamma = \arctan(|E_{\phi_r}|/|E_{\theta_r}|)$ and δ is the phase difference between the reflected components.

Following the condition in (1), the groove period was fixed at 1.1 mm, while the depth was optimized considering the observations in [33]. This optimization yielded an optimal depth of 0.46 mm. According to (25) and the definition provided in γ, when designing an elliptical polarizer with the optimal range of variation in ellipticity β, it is imperative that the phase change τ corresponds to $3/2\pi$ for $\tan(\Phi) = \pm(1/\cos\theta)$. By using the proposed numerical program, it was possible to quickly determine the optimal corrugation depth for the sinusoidal profile that maximizes the performance of the elliptical polarizer. Specifically, for a rotation angle of 47.27°, the resulting phase difference is approximately 272°, which is very close to the target value.

After optimizing the depth and period of the chosen sinusoidal profile, it was possible, using the program we developed, to obtain the value of the phase shift τ as function of the rotation angle Φ (Fig. 5). By analyzing the phase shift obtained, and considering (23), we were able to evaluate the performances of the polarizar in terms of rotation angle α and ellipticity β. Specifically, our goal was to ensure that the range of variation for the parameter β was as wide as possible, allowing all the output polarization states to be achieved. As can be seen in the graph in Fig. 6, the maximum ellipticity achievable by our elliptical polarizer is very close to the theoretical value of 45 degrees. Specifically, we obtain a maximum value β of 44 degrees.

4. Electromagnetic simulation

After studying the behavior of the single elliptical polarizer, taking into account diffraction theory, it was necessary to assess the results obtained through electromagnetic simulations. The software chosen for this verification was the commercial High-Frequency Structure Simulator (Ansys HFSS [34]). Since the structure of the polarizer is periodic, for the electromagnetic simulation, it was sufficient to consider a single period of the corrugation. With the appropriate Primary/Secondary boundaries, it was then possible to model the periodic structure [35]. The Unit Cell modeled in the HFSS software is shown in Fig. 7. The objective of this simulation was to extract information about the electric field reflected by the Unit Cell to determine the phase difference τ and compare it with the numerical results obtained with our developed

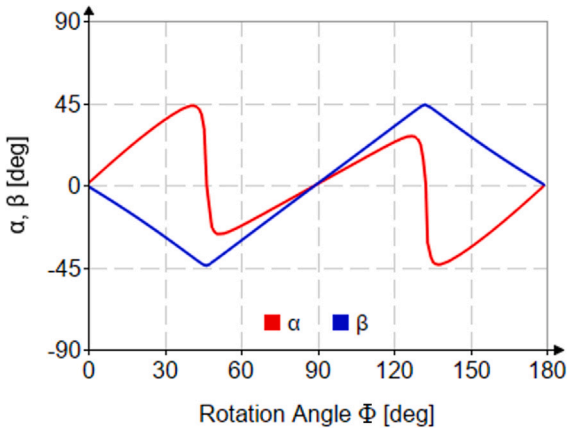

Fig. 6. Rotation angle α and ellipticity β of the polarization as function of the rotation angle Φ of the polarizer calculated with our mathematical program.

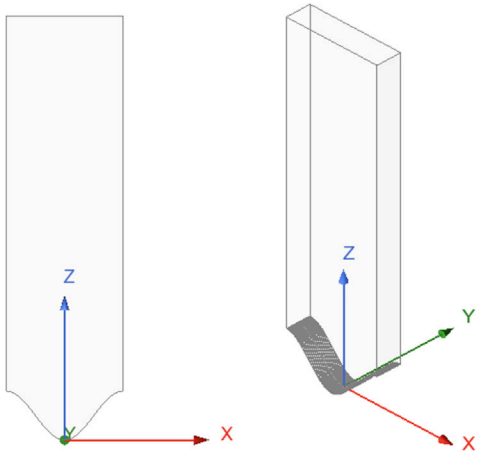

Fig. 7. Unit Cell of the elliptical polarizer in HFSS.

program. The Unit Cell was excited by inserting a Floquet port at the upper end of the structure box. The Floquet port is a type of excitation used exclusively for simulating planar periodic structures and allows for analyzing a single period and then extrapolating the behavior of the entire infinite periodic structure. The material for the corrugation is considered as PEC (Perfect Electric Conductor), while the material chosen for the structure containing the corrugation, on the other hand, is vacuum. Additionally, we set up the simulation in such a way that the corrugation could rotate in the xy plane; For this reason, we defined a rotation angle Φ and carried out a parametric simulation. This choice thus allowed for a clearer and more meaningful comparison with the results obtained from the analytical approach.

By analyzing the magnitude and phase of the S parameters obtained from HFSS and applying (16) and (23), the simulated phase difference τ was determined as a function of the rotation angle Φ. A comparison between the results obtained using our analytical model and those derived from full-wave electromagnetic simulations is presented in Fig. 8.

The analytical and simulation results show excellent agreement, with a maximum relative error of approximately 0.5% in the worst-case scenario.

5. Combination of the two polarizer mirrors

As discussed previously, in order to realize a universal polarizer, it is necessary to combine two polarizers. In the DTT's specific case

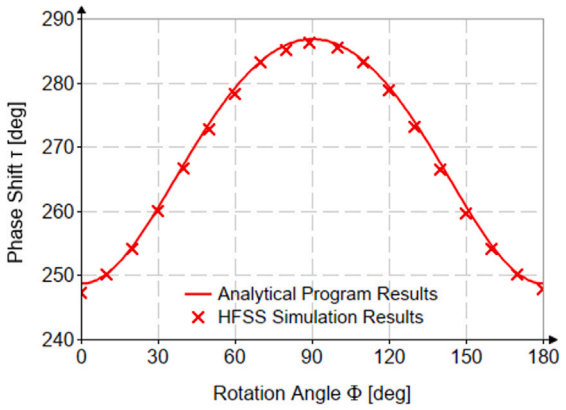

Fig. 8. Comparison between analytical and simulation results for the computation of the phase shift τ as a function of the rotation angle Φ.

considered here, the two polarizers share identical geometrical characteristics and operate at the same angle of incidence. In addition, the incident and reflected wave vectors are on the same plane. To account for all possible output polarization states, the interaction between the two polarizers must be modeled using a matrix-based approach. In the case of a system composed of two elliptical polarizers, the reflected electric field can be expressed as follows:

$$\begin{bmatrix} E_{\theta r} \\ E_{\phi r} \end{bmatrix} = \begin{bmatrix} \cos\frac{\tau_2}{2} + i\sin\frac{\tau_2}{2}\cos 2\xi_2 & -i\sin\frac{\tau_2}{2}\sin 2\xi_2 \\ i\sin\frac{\tau_2}{2}\sin 2\xi_2 & -\cos\frac{\tau_2}{2} + i\sin\frac{\tau_2}{2}\cos 2\xi_2 \end{bmatrix} \begin{bmatrix} \cos\frac{\tau_1}{2} + i\sin\frac{\tau_1}{2}\cos 2\xi_1 & -i\sin\frac{\tau_1}{2}\sin 2\xi_1 \\ i\sin\frac{\tau_1}{2}\sin 2\xi_1 & -\cos\frac{\tau_1}{2} + i\sin\frac{\tau_1}{2}\cos 2\xi_1 \end{bmatrix} \begin{bmatrix} E_{\theta i} \\ E_{\phi i} \end{bmatrix} \tag{26}$$

where ξ_1, τ_1 represent the parameters of the first elliptical grating polarizer and ξ_2, τ_2 represent the parameters of the second elliptical grating polarizer. In our case, since the two polarizers are identical, the phase shift values (denoted τ_1 and τ_2) are the same for both elements.

Using the proposed mathematical model, we generated key contour plots that are essential to understanding the behavior of the polarizers. These plots offer a comprehensive representation of the achievable polarization states as a function of the rotation angles of the two polarizers. The graphs were obtained by assuming a ($E_{\theta i}$ = 1, $E_{\phi i}$ = 0) incident polarization on the first polarizer. The contour plots derived from our analytical model are shown in Figs. 9 and 10. Fig. 9 shows the possible combinations of the polarization rotation angle (α) at the output of the system as a function of the mechanical rotation angles of the two polarizers (Φ_1 and Φ_2), while Fig. 10 shows the corresponding combinations of the output polarization ellipticity (β), also as a function of the mechanical rotation angles of the polarizers (Φ_1 and Φ_2). Assuming a priori knowledge of the polarization required to ensure proper plasma matching, the two contour plots provide a direct reference for determining the optimal mechanical configurations of the polarizers necessary to achieve this condition.

5.1. Calculation of polarization purity

After calculating the possible combinations of α and β that can be obtained by combining the two designed polarizers, it was necessary to consider a quantity known as polarization purity [36]. This quantity allows for the evaluation of whether all possible state combinations (α_p, β_p) can be realized with the pair of polarizers and, if so, with what efficiency. The polarization purity η is defined as:

$$\eta = \cos^2(\alpha_p - \alpha_c)\cos^2(\beta_p - \beta_c) + \sin^2(\alpha_p - \alpha_c)\sin^2(\beta_p + \beta_c) \tag{27}$$

When η=1, it means that the two polarization states are identical, whereas when η=0, the two polarization states are orthogonal. In the

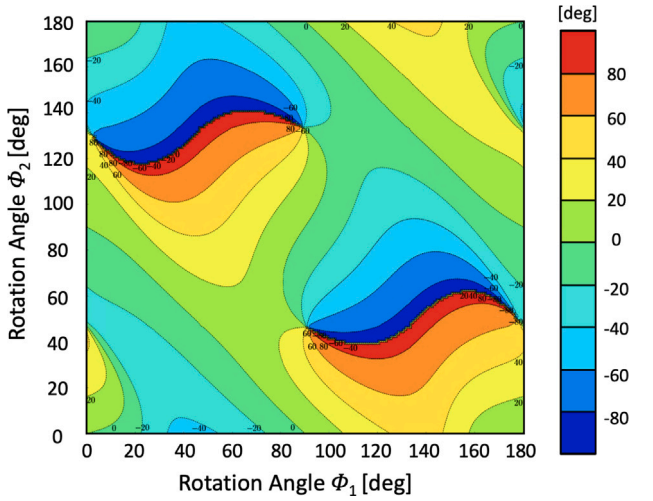

Fig. 9. Rotation angle α as a function of the mechanical rotation angles of the two polarizers (Φ_1 and Φ_2).

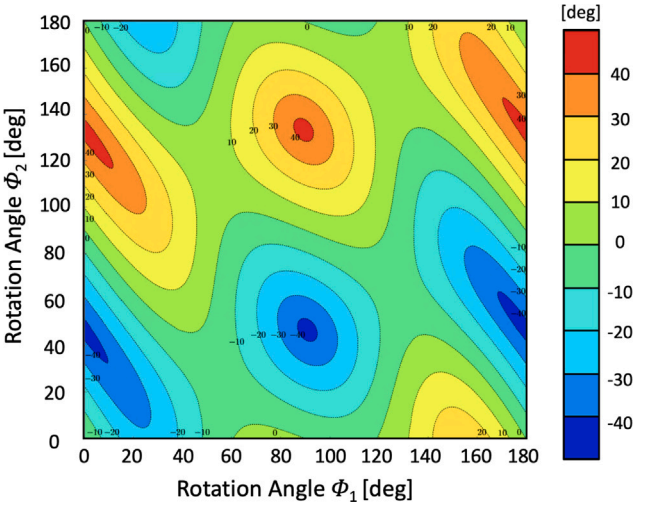

Fig. 10. Ellipticity β as a function of the mechanical rotation angles of the two polarizers (Φ_1 and Φ_2).

previous equation, α_c and β_c correspond to the rotation angle and ellipticity values calculated with our program, while α_p and β_p are the values corresponding to any possible combination. After implementing the formula in the program, we obtained a new contour plot (Fig. 11), which illustrates the polarization purity as a function of the desired parameter combinations.

The minimum calculated value of η is equal to 99.94%. This result indicates that, with the chosen setup, it is possible to realize all the combinations of the parameters α and β within the selected range. Consequently, this ensures the capability to generate any desired polarization state of the electric field at the output of the transmission line.

6. Discussions

The results of the program discussed in this paper should be compared with similar results that could be obtained using commercial Computer-Aided Design (CAD) software. Computation efficiency is a very important parameter that has to be considered when performing a general design. In this context, the developed program avoids the need to draw a full three-dimensional model and select boundary conditions required by electromagnetic CAD software for highly accurate simulations. Moreover, even for generating advanced graphical outputs, such as contour plots, no post-processing is required, an operation that is instead mandatory when adopting a simulation-based approach. Moreover, the scale of the problem, specifically the disparity between the wavelength and the mirror dimensions, makes full-system simulations unfeasible, whereas the analytical approach presented in the paper bypasses this limitation, offering significant flexibility in terms of geometries, applications, and number of components. However, the present model assumes perfect periodicity, ideal conductive materials, and neglects any thermal deformation and fabrication tolerances. In real-world applications, these effects could slightly alter the behavior of the polarizers, particularly at high operating powers. Future experimental validation on prototype polarizers will be crucial to quantify such deviations and assess the robustness of the design under realistic operating conditions.

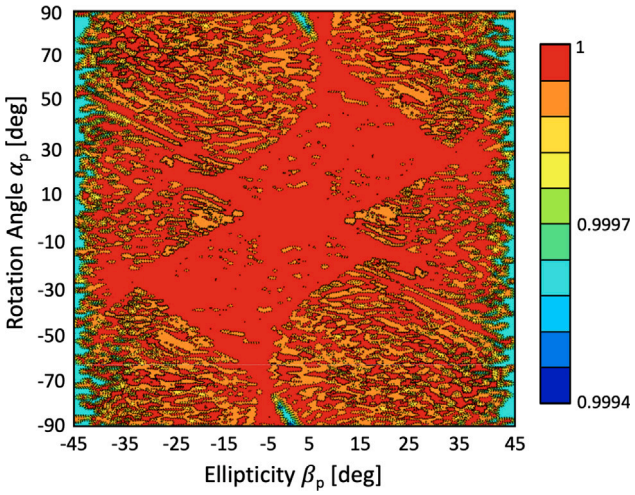

Fig. 11. Polarization purity η as a function of all the possible polarization states. α_p and β_p represent, respectively, the rotation angle and ellipticity of the desired polarization.

7. Conclusions

This paper presented the analytical modeling, design, and verification of a sinusoidal grating elliptical polarizer and its application for the 170 GHz Electron Cyclotron Resonance Heating (ECRH) system of the Divertor Tokamak Test (DTT) facility. The analytical program, described in this work, allows for the accurate computation of the phase shift introduced by the grooves of the polarizer and to analyze the polarization properties of the reflected electric field for arbitrary corrugation profiles and design parameters, such as frequency and angle of incidence. Moreover, the developed program enables the calculation of the phase shift (τ) and the polarization characteristics of a single polarizer or two combined polarizers, avoiding the need for a 3D model or post-processing requirements typically associated with the use of electromagnetic simulation software. The analytical predictions were validated by full-wave electromagnetic simulations using HFSS with a maximum relative error of approximately 0.5%. With the proposed method, it is possible to calculate the optimal corrugation depth to be employed to maximize ellipticity and study any possible polarization variation. Moreover, the combination of two identical elliptical polarizers was theoretically shown to give full control over the output state of polarization, in terms of rotation angle and ellipticity. The output contour plots are a convenient map of the mechanical rotation angles required in order to achieve any given output polarization and

to ensure efficient coupling to the plasma. The optimized analysis tool offers a secure and efficient approach to polarizer design and optimization in high-power ECRH systems and could be integrated into routine systems engineering tasks for plasma applications in nuclear fusion.

CRediT authorship contribution statement

Sofia Bertolami: Writing – review & editing, Writing – original draft, Validation, Methodology, Investigation, Formal analysis, Conceptualization. **Franco Di Paolo:** Supervision, Investigation, Formal analysis, Conceptualization. **Alessandro Bruschi:** Writing – review & editing, Supervision, Methodology, Investigation, Formal analysis. **Francesco Fanale:** Writing – review & editing, Supervision, Methodology, Investigation, Formal analysis. **Alessandro Moro:** Writing – review & editing, Supervision, Methodology, Investigation, Formal analysis. **Saul Garavaglia:** Writing – review & editing, Supervision, Methodology, Investigation, Formal analysis. **Gustavo Granucci:** Writing – review & editing, Supervision, Methodology, Investigation, Formal analysis. **Afra Romano:** Writing – review & editing, Supervision, Methodology, Investigation, Formal analysis. **Alessandro Simonetto:** Writing – review & editing, Supervision, Methodology, Investigation, Formal analysis.

Declaration of competing interest

The authors declare that they have no known competing financial interests or personal relationships that could have appeared to influence the work reported in this paper.

Data availability

No data was used for the research described in the article.

References

[1] European Commission website, Consequences of climate change, 2025, https://climate.ec.europa.eu/climate-change/consequences-climate-change-en. (Accessed 24 July 2025).

[2] United Nation website, Causes and effects of climate change, 2025, https://www.un.org/en/climatechange/science/causes-effects-climate-change. (Accessed 24 July 2025).

[3] F. Romanelli, on behalf of DTT Contributors, Divertor tokamak test facility project: status of design and implementation, Nucl. Fusion 64 (11) (2024) 112015, http://dx.doi.org/10.1088/1741-4326/ad5740.

[4] S. Garavaglia, B. Baiocchi, A. Bruschi, D. Busi, F. Fanale, L. Figini, G. Granucci, A. Moro, P. Platania, N. Rispoli, A. Romano, A. Salvitti, E. Sartori, S. Schmuck, E. Vassallo, Progress of DTT ECRH system design, Fusion Eng. Des. 168 (2021) 112678, http://dx.doi.org/10.1016/j.fusengdes.2021.112678.

[5] G. Granucci, F. Auriemma, L. Aucone, B. Baiocchi, N. Bonanomi, F. Braghin, A. Bruschi, D. Busi, I. Casiraghi, L.E. di Grazia, F. Fanale, L. Figini, S. Garavaglia, P. Mantica, M. Mattei, A. Moro, S. Nowak, P. Platania, D. Ricci, N. Rispoli, A. Romano, G. Rubino, S. Schmuck, A. Simonetto, Roles of ECH system in DTT plasma operations, Nucl. Fusion 64 (12) (2024) 126036, http://dx.doi.org/10.1088/1741-4326/ad7742.

[6] S. Garavaglia, L. Balbinot, A. Bruschi, D. Busi, A. Bussolan, F. Fanale, G. Granucci, A. Moro, P. Platania, N. Rispoli, A. Romano, E. Sartori, S. Schmuck, A. Simonetto, E. Vassallo, Development of the electron cyclotron resonance heating system for divertor tokamak test, J. Vac. Sci. Technol. B 41 (4) (2023) 044201, http://dx.doi.org/10.1116/6.0002396.

[7] R. Temkin, V. Granatstein, G. Nusinovich, Introduction to the Physics of Gyrotrons, Johns Hopkins University Press, 2004.

[8] M. Thumm, State-of-the-art of high-power gyro-devices: 2025 update of experimental results, J Infrared Milli Terahz Waves 46 (2025) http://dx.doi.org/10.1007/s10762-025-01042-y.

[9] N. Kumar, U. Singh, A. Bera, A.K. Sinha, A review on the sub-THz/thz gyrotrons, Infrared Phys. Technol. 76 (2016) 38–51, http://dx.doi.org/10.1016/j.infrared.2016.01.015.

[10] M. Ćwikliński, P. Brückner, S. Leone, C. Friesicke, H. Maßler, R. Lozar, S. Wagner, R. Quay, O. Ambacher, D-band and G-band high-performance GaN power amplifier MMICs, IEEE Trans. Microw. Theory Tech. 67 (12) (2019) 5080–5089, http://dx.doi.org/10.1109/TMTT.2019.2936558.

[11] F. Guo, Y. Xu, S. Wu, H. Tao, E. Ma, T. Chen, W. Wang, 100 mw G-band MMIC power amplifier based on 50nm GaN hemt technology, in: 2022 Photonics & Electromagnetics Research Symposium, PIERS, 2022, pp. 748–751, http://dx.doi.org/10.1109/PIERS55526.2022.9793013.

[12] D. Passi, A. Leggieri, F. Di Paolo, M. Bartocci, A. Tafuto, A. Manna, High efficiency ka-band spatial combiner, AEM 3 (2014) http://dx.doi.org/10.7716/aem.v3i2.267.

[13] S. Fantauzzi, L. Valletti, F. Di Paolo, High power density spatial combiner for the Q-band, ready for space applications, Prog. Electromagn. Res. M 109 (2022) 163–177, http://dx.doi.org/10.2528/PIERM21120903.

[14] D. Passi, A. Leggieri, F. Di Paolo, A. Tafuto, M. Bartocci, Spatial power combiner technology, in: Progress in Electromagnetics Research Symposium, 2015.

[15] D. Passi, A. Leggieri, F. Di Paolo, M. Bartocci, A. Tafuto, Design of high power density amplifiers: Application to ka band, J Infrared Milli Terahz Waves 38 (10) (2017) 1252–1263.

[16] J. Benford, J. Swegle, E. Schamiloglu, High Power Microwaves, CRC Press, 2007.

[17] S. Bertolami, L. Valletti, S. Fantauzzi, F. Di Paolo, M. Bartocci, P. Bia, A. Manna, Comprehensive analysis of a slow wave structure for an X-band MILO, in: Photonics & Electromagnetics Research Symposium (PIERS), 2023, pp. 1652–1660, http://dx.doi.org/10.1109/PIERS59004.2023.10221358.

[18] L. Valletti, S. Fantauzzi, F. Di Paolo, Innovative mode enhancement for high power coaxial vircators, IEEE Trans. Electron Devices 70 (7) (2023) 1–8, http://dx.doi.org/10.1109/TED.2023.3274497.

[19] N. Vinokurov, Free electron lasers as a high-power terahertz sources, J Infrared Milli Terahz Waves 32 (2011) 1123–1143, http://dx.doi.org/10.1007/s10762-011-9766-9.

[20] Y. Socol, High-power free-electron lasers–technology and future applications, Opt. Laser Technol. 46 (2013) 111–126, http://dx.doi.org/10.1016/j.optlastec.2012.06.040.

[21] W.H. Urbanus, W.A. Bongers, V. Bratman, C.A.J. van der Geer, M.F. Graswinckel, P. Manintveld, B.L. Militsyn, A Savilov, Long-pulse operation at constant output power and single-frequency mode of a high-power electrostatic free-electron maser with depressed collector, Phys. Rev. Lett. 89 (2002) 214801, http://dx.doi.org/10.1103/PhysRevLett.89.214801.

[22] F. Fanale, A. Bruschi, S. Garavaglia, A. Moro, B. Baiocchi, M. Bonesso, F. Braghin, D. Busi, R. Dima, P. Fanelli, L. Figini, E. Gajetti, G. Granucci, D. Mascali, S. Passarello, A. Pepato, P. Platania, P. Rebesan, A. Romano, A. Salvitti, L. Savoldi, A. Simonetto, S. Schmuck, G. Torrisi, M. Turcato, Status of DTT ech transmission lines and antennae, IEEE Trans. Plasma Sci. 52 (9) (2024) 3778–3784, http://dx.doi.org/10.1109/TPS.2024.3382745.

[23] A. Moro, A. Bruschi, F. Fanale, P. Fanelli, E. Gajetti, S. Garavaglia, G. Granucci, S. Meloni, A. Pepato, P. Platania, A. Romano, A. Salvitti, L. Savoldi, S. Schmuck, M. Scungio, A. Simonetto, M. Turcato, E. Vassallo, Progress and challenges of the ECH transmission line design for DTT, Fusion Eng. Des. 202 (2024) 114391, http://dx.doi.org/10.1016/j.fusengdes.2024.114391.

[24] F. Leuterer, D. Wagner, J. Stober, W. Kasparek, C. Lechte, ASDEX Upgrade Team, Experimental study of ohmic losses of polarizer mirror system, EPJ Web Conf. 149 (2017).

[25] J.L. Doane, Grating polarizers in waveguide miter bends, J Infrared Milli Terahz Waves 13 (1992) 1727–1743.

[26] Y.L. Kok, N.C. Gallagher, Relative phases of electromagnetic waves diffracted by a perfectly conducting rectangular-grooved grating, J. Opt. Soc. Amer. A 5 (1) (1988) 65–73, http://dx.doi.org/10.1364/JOSAA.5.000065.

[27] T. Antonakakis, F. Baida, A. Belkhir, K. Cherednichenko, S. Cooper, R. Craster, G. Demésy, J. Desanto, G. Granet, B. Gralak, S. Guenneau, D. Maystre, A. Nicolet, B. Stout, F. Zolla, B. Vial, E. Popov, Gratings: Theory and Numeric Applications, Presses Universitaires de Provence, 2012.

[28] K. Nagasaki, Y. Itoh, K. Sakamoto, T. Obiki, T. Maekawa, H. Morioka, T. Terumichi, M. Asakawa, M. Shats, H. Punzmann, Polarizers with non-rectangular grooves for high power millimeter waves, Fusion Eng. Des. 53 (2001) 491–497, http://dx.doi.org/10.1016/S0920-3796(00)00525-1.

[29] L. Li, J. Chandezon, G. Granet, J. Plumey, Rigorous and efficient grating-analysis method made easy for optical engineers, Appl. Opt. 38 (2) (1999) 304–313, http://dx.doi.org/10.1364/AO.38.000304.

[30] C. Tsai, S. Wu, Study of broadband polarization conversion with metallic surface-relief gratings by rigorous coupled-wave analysis, J. Opt. Soc. Amer. A 25 (2008) 1339–1348, http://dx.doi.org/10.1364/JOSAA.25.001339.

[31] D. Xia, M. Huang, Z. Wang, F. Zhang, G. Zhuang, Integral staggered point-matching method for millimeter-wave reflective diffraction gratings on electron cyclotron heating systems, Fusion Eng. Des. 108 (2016) 55–59, http://dx.doi.org/10.1016/j.fusengdes.2016.04.038.

[32] PTC, PTC Mathcad Prime. Version 10.0. https://www.ptc.com/en/products/mathcad.

[33] F. Zhang, M. Huang, D. Xia, S. Song, J. Wang, B. Huang, H. Wang, Study of the polarization strategy for electron cyclotron heating systems on HL-2M, J Infrared Milli Terahz Waves 37 (2016) http://dx.doi.org/10.1007/s10762-016-0245-1.

[34] Ansys Inc., ANSYS HFSS (High Frequency Structure Simulator), Version 2023 R2. https://www.ansys.com/products/electronics/ansys-hfss.

[35] H.M. Hoffmann, S.K. Jawla, M.A. Shapiro, G. Hanson, R.J. Temkin, Grating polarizers at 170 GHz for ECRH systems: Low power tests and simulations, IEEE Trans. Antennas and Propagation 66 (9) (2018) 4719–4728, http://dx.doi.org/10.1109/TAP.2018.2851377.

[36] T. Ii, S. Kubo, T. Shimozuma, S. Kobayashi, K. Okada, Y. Yoshimura, H. Igami, H. Takahashi, S. Ito, Y. Mizuno, K. Okada, R. Makino, K. Kobayashi, Y. Goto, T. Mutoh, Design of polarizers for a mega-watt long-pulse millimeter-wave transmission line on the large helical device, Rev. Sci. Instrum. 86 (2) (2015) 023502, http://dx.doi.org/10.1063/1.4907355.